International Journal of Multiphase Flow 36 (2010) 349–363

Contents lists available at ScienceDirect

International Journal of Multiphase Flow

journal homepage: www.elsevier.com/locate/ijmulflow

Drop size spectra in sprays from pressure-swirl atomizers

Andreas Tratnig, Günter Brenn *

Institute of Fluid Mechanics and Heat Transfer, Graz University of Technology, Inffeldgasse 25/F, 8010 Graz, Austria

ARTICLE INFO

Article history:
Received 7 October 2009
Received in revised form 7 December 2009
Accepted 22 January 2010
Available online 2 February 2010

Keywords:
Conical sheet atomization
Sauter mean drop size
Drop size spectrum
Gamma distribution

ABSTRACT

A study on the characterization of sprays from Newtonian liquids produced by pressure-swirl atomizers is presented. The global drop size spectra of the sprays are measured with phase-Doppler anemometry, and global mean drop sizes are derived as moments of the spectra for varying atomizer geometry, liquid flow rate, and physical properties of the liquids. Dimensional analysis provides a correlation for the non-dimensional global Sauter mean diameter. A relationship between the global Sauter mean drop size and the global drop size RMS is established. A method is developed for predicting the global drop size spectra in the sprays, using easily accessible experimental input parameters. The basis for the function defining the spectrum is a gamma distribution, which is known from the literature as physically relevant for ligament-mediated sprays.

1. Introduction

Liquid sprays produced by pressure atomizers are important for many technical processes, such as energy conversion, coating, and cooling, to name but a few. A group of widely used pressure atomizers are the pre-filming atomizers, which turn the emerging liquid into sheets propagating from the atomizer orifices. The flat fan-shaped or conical sheets break up into droplets due to the Kelvin–Helmholtz instability, which leads to ligament formation, and due to the capillary instability of the ligaments, which forms the final droplets. Due to the wide use of this type of atomizers, researchers have been investigating since decades the spray drop ensembles resulting from the sheet break-up as functions of the influencing parameters. The highest detail of information on a spray drop ensemble is represented by the spectra of the drop size and velocity. It has been an aim of spray research since a long time to find a reliable way of modeling and/or predicting at least the spectrum of the drop size produced by sheet break-up, since this spectrum influences most transport properties of the spray relevant to the technical process. It is the aim of the present work to provide a reliable prediction of the spray drop size spectrum as produced by the break-up of conical sheets from pressure-swirl atomizers.

Starting from the pioneer work by Squire (1953), many researchers analyzed the stability behavior of parallel-sided or attenuating liquid sheets in their gaseous environments (e.g., Dombrowski and Johns, 1963; Clark and Dombrowski, 1972; Li and Tankin, 1991; Senecal et al., 1999). These works concentrate on determining the wavelength and growth rate of the most unstable ("optimum") disturbance. The optimum wavelength, together with the sheet thickness at break-up, determines the resultant diameter of ligaments detached from the sheets. The second step is to deduce a representative drop size, assuming break-up of the ligaments by the mechanism analyzed theoretically by Weber (1931). The so obtained drop size is interpreted as a Sauter mean drop size in the spray. The drop sizes from the model calculation and from measurements, however, often do not agree very well (Dombrowski and Johns, 1963).

The stability analysis, as well as experimental investigations, show that physical properties of the liquid, such as density, dynamic viscosity, and surface tension against the ambient medium, influence the drop size resulting from the two-step model break-up process. It is seen that the break-up length of the sheet and the Sauter mean drop size increase with the liquid dynamic viscosity (e.g., Nonnenmacher and Piesche, 2000). Experimental investigations on the atomization of liquid sheets from pre-filming pressure atomizers showed that the mean drop sizes in the spray increase with the surface tension of the liquid against the ambient medium. This effect is due to a shift of the entire drop size spectrum towards larger diameters. An increase of the liquid dynamic viscosity also leads to larger mean drop sizes, but due to a selective increase of numbers of large drops (Dorfner et al., 1995). Bremond et al. (2007) showed that the wavelengths of the dominant waves are influenced by surface tension and density of the liquid. In non-Newtonian liquids, such as water-in-oil emulsions, it is seen that an increase of the aqueous phase concentration leads to larger Sauter mean drop sizes when atomizing liquid jets (Sheng et al., 2006). At low injection pressures, an increase of the Sauter mean diameter by more than 70% may result from turning Diesel fuel into

* Corresponding author. Tel.: +43 316 873 7341; fax: +43 316 873 7356.
E-mail address: brenn@fluidmech.tu-graz.ac.at (G. Brenn).

0301-9322/$ - see front matter © 2010 Elsevier Ltd. All rights reserved.
doi:10.1016/j.ijmultiphaseflow.2010.01.008

a water-in-oil emulsion with an aqueous phase concentration of 50%. The degree of increase depends on the emulsifier used. The same trend was seen in the data for flat-fan sheet break-up by Miller and Butler Ellis (2000), Dexter (2001), and Hewitt (2008). The non-Newtonian flow behavior of suspensions, e.g., of lime in water, raises the resulting drop size (Schütz et al., 2004). Overall, what is best investigated as liquid properties influencing the drop size spectrum in sprays are the surface tension against air and the dynamic viscosity. However, detailed information about the quantitative influences of these parameters is missing in the literature.

What is most important for the characterization of a spray for most applications is the drop size spectrum. The velocity spectrum is easily changed by influences from the ambient air and, therefore, not equally important as a primary property of the spray. It has been the subject of research since a long time to find an appropriate mathematical function that characterizes the drop size spectra of sprays. There exist two different approaches: the first one uses mathematical functions assumed suitable for representing the shapes of the spectra. The functions typically depend on two to four free parameters, and their values are determined by fitting the function to experimental data (Mugele and Evans, 1951; Xu et al., 1993; Bhatia and Durst, 1989; Paloposki, 1994). Since this approach is quite heuristic, the alternative approach of using physically based functions for representing the drop size spectra seems more attractive. One such function is obtained by the maximum-entropy formalism, maximizing the Shannon entropy under constraints from the conservation equations (e.g., Sellens and Brzustowski, 1985; Li and Tankin, 1989; Babinsky and Sojka, 2002; Dumouchel, 2006). The agreement of modeled and measured drop size spectra shown in these papers is satisfactory. However, the deviations between model and experiment seen in the published data indicate an inaccuracy of the moments of the spectra which is unacceptable in view of the aims of the present work. An alternative emerges from the model assumption that drops in ligament-mediated sprays are produced by coalescence of liquid blobs which make up the ligaments (Villermaux et al., 2004). This model leads to a function for the drop size spectrum which involves the gamma function and is therefore called a gamma distribution (Marmottant and Villermaux, 2004; Bremond et al., 2007; Villermaux, 2007). Basically the same kind of function is obtained by Dumouchel (2006) using a new formulation of the maximum-entropy formalism.

The approach with the gamma distribution is favored in the present context and used for predicting the drop size spectra in hollow-cone sprays on the basis of experimental data. The paper is organized as follows: the next section presents experiments carried out for characterizing the drop sizes in sprays from pressure-swirl atomizers. Section 3 presents the experimental results by a universal non-dimensional equation. In Section 4 we show that the approach to represent the measured mean spray drop sizes with the Dombrowski and Johns model leads to unsatisfactory results. As an alternative, Section 5 develops a modified gamma distribution as a function to predict the drop size spectra accurately enough to represent their moments well. In Section 6 the conclusions from the work are drawn.

2. Experiments on sprays from pressure-swirl atomizers

2.1. The test rig

The experiments were carried out using the test rig sketched in Fig. 1. This rig consists of a spray box, a low-pressure and a high-pressure pump, the tubing, a spray nozzle, an exhaust ventilation, and devices for process monitoring as well as drop size and velocity measurements. The rig can be run in two operational modes: the closed-loop mode, which uses the intercepting tank of the spray box both for collecting the atomized test liquid and for storing it; and the open-loop mode, which uses the tank of the spray box to collect the atomized liquid, and a different tank for storing the test liquid to be sprayed. In both cases, the liquid is pumped with the help of a low-pressure pump to the Coriolis mass flow meter Foxboro CFS 10, where, further to the mass flow rate, the liquid density and temperature are measured. The high-pressure pump feeds the atomizer. The liquid is sprayed into the spray box, where it is collected in both operational modes. The exhaust ventilation suppresses spray drop recirculation, which would disturb the measurements of the spray properties. The position of the atomizer may be changed by means of the two-axes traverse. The necessity to change the position of the atomizer arises from the local nature of the PDA measuring technique used for characterizing the spray flow.

For the experiments of the present study, the open-loop operation mode of the rig was chosen, since the test liquids used for the experiments were mixtures with volatile components, which tend to evaporate during the measurements, thus changing the composition of the mixtures. The consequence would be measurements with continuously changing liquid properties. The open-loop mode ensures the atomization of liquids with constant (and well defined) physical properties, and therefore ensures well defined experimental conditions.

The atomizers used in the experiments were Delavan SDX pressure-swirl atomizers. They consist of a swirl chamber, an end plate, and an orifice disk, as sketched in Fig. 2 (sketch by Nestlé Product Technology Centre Konolfingen, Switzerland). The swirl chambers used in the study were types SB, SC, SD, and SF, each with a single

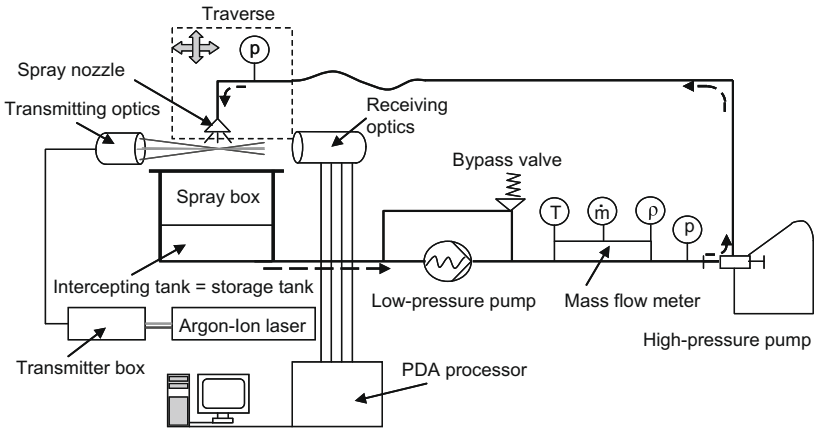

Fig. 1. Sketch of the spray test rig.

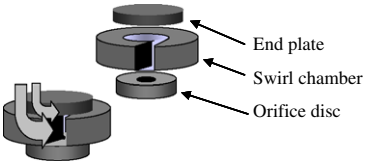

Fig. 2. Sketch of the Delavan SDX atomizer. The liquid enters the swirl chamber through the single inlet slit (sketch by Nestlé Product Technology Centre Konolfingen).

Table 1
Dimensions of the Delavan SDX swirl chambers.

Swirl chamber type	Swirl chamber height h_{SC} (mm)	Swirl chamber diameter d_{SC} (mm)	Swirl chamber inlet width b_{Ch} (mm)
SB	1.23	11.85	1.61
SC	1.36	10.71	2.45
SD	1.88	10.71	2.45
SF	3.77	10.71	2.45

Table 2
Exit hole diameters in the Delavan SDX orifice plates.

Orifice type (–)	Orifice diameter d_{Or} (mm)
30	0.762
40	1.016
50	1.270
60	1.524
70	1.778

inlet slit. The values of the swirl chamber diameter d_{SC} and height h_{SC}, and the inlet slit width b_{Ch}, are summarized in Table 1. Orifice plates with different exit hole diameters, termed types 30, 40, 50, 60, and 70, were used. The type numbers denote the orifice hole diameter d_{Or} in thousandths of an inch. The hole diameters in mm are listed in Table 2. The uniform orifice plate thickness is 3.16 mm, and the inlet curvature radius is 1.85 mm throughout. Thus, the cylindrical section of the orifice has a length of 1.31 mm in all orifice plates. Since the swirl chambers may be combined flexibly with the orifice plates, there is a wide geometric variability of the atomizers.

2.2. Techniques for characterizing the spray flows

The present series of experiments on the formation of sprays from pressure-swirl atomizers aimed at a detailed characterization of the sprays. Two important global geometrical parameters, the sheet opening angle and the sheet break-up length, were determined from photographs of the sprays by simple image processing (see Fig. 3). The photographs were taken with a digital camera, using flashlight illumination from the front in order to have reliable images for determining the sheet break-up length. Furthermore, the mean drop sizes in the sprays, especially the global number mean and Sauter mean drop sizes, $D_{10,global}$ and $D_{32,global}$, were determined as functions of the various influencing quantities. The global Sauter mean drop size represents a drop with the same volume to surface area ratio as the entire spray. It is thus an important quantity for characterizing the atomization process for applications with transfer processes across the drop surface. The measurement of properties of the spray drops requires a measuring technique such as the light diffraction-based Malvern technique or phase-Doppler anemometry (PDA). The advantage of the latter is that it provides local information about the spray drops

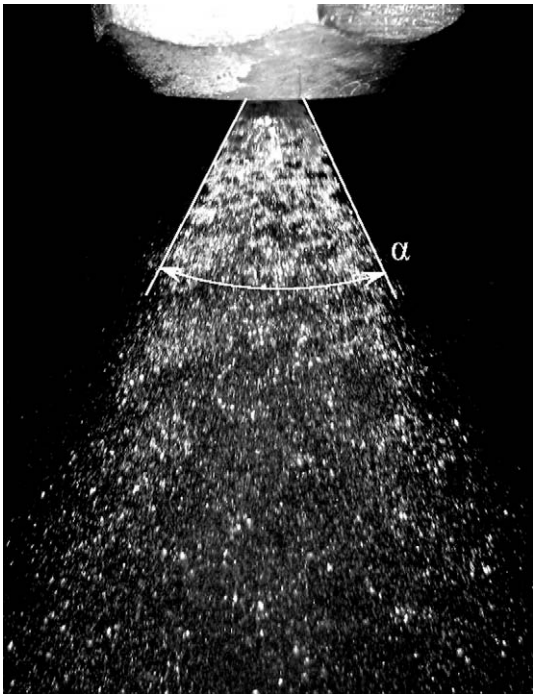

Fig. 3. Photograph of a water spray with the conical sheet opening angle α, produced by the spray nozzle type SC-30 at the mass flow rate of 20.8 kg/h (corresponding driving pressure difference: 7 bar).

with high resolution, so that PDA was chosen for the present study. Global spray properties are derived from the local PDA data by a post-processing routine, which will be discussed below.

A phase-Doppler anemometer measures size and velocity of drops passing an optically defined probe volume. The laser light source of the present DANTEC PDA system is a continuous-wave Argon-Ion laser Coherent Innova 90C-3. The probe volume of the present standard PDA system is formed by the intersection of four laser beams, depicted as grey lines in Fig. 1. The diameter and velocity measurement bases on the analysis of laser light scattered from the probe volume by the spray drops. The refracted and reflected components of the scattered light may be used for PDA. The dominance of one of these two scattering modes, which is a prerequisite for correct PDA measurements, is determined by the optical configuration of the PDA system and the refractive index of the drop liquid. An important parameter of the optical configuration of the PDA system is the off-axis angle (scattering angle) φ where the receiving optics unit is placed (see Fig. 4). The liquids

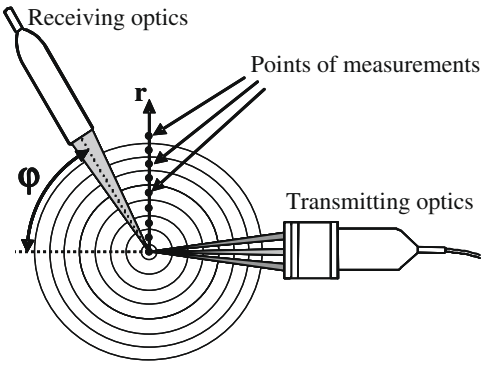

Fig. 4. Sketch of a spray cross section with the points of measurements and the transmitting and receiving optics units of the PDA system. The points of measurement are equidistant.

used in the present investigations are optically transparent water–sucrose–ethanol solutions. As a consequence of this, the dominant scattering mode chosen was the refractive mode, which yields high scattered light intensities in forward directions. The appropriate scattering angle for this mode was 50° in all measurements. The phase factor relating the drop size to the Doppler signal phase shift was −0.575°/μm throughout. The maximum measurable drop size was 450.9 μm. The optical signals are converted into electrical signals by the photodetectors. For the signal and data processing, the Dantec PDA processor 58N50 and the Dantec BSA Flow Software in the version 2.12 were used.

For obtaining global spray properties, local drop ensembles were measured with the PDA at 31 points in each spray cross section. The distance of the plane of measurement from the atomizer orifice was 80 mm in all measurements. This distance was found by visualization of the drops as the best compromise for the measurements of all experiments, closest possible to the sheet breakup zone to ensure that the measurements capture the drop formation process only, without a notable influence from evaporation and coalescence, and still ensuring spherical drops for the PDA measurements. The points of measurement were arranged equidistant along one radius of the cross section, as sketched in Fig. 4. Axial symmetry of the sprays was verified in preliminary tests. The outermost point was determined by the condition that the frequency of drop arrival at the probe volume (the data rate) there should be 30 Hz. The distance between the points of measurement varied between the different sprays. Sufficient statistical reliability of the PDA measurement results was ensured by acquiring 20,000 drops in each local measurement.

For every local measurement, the drop sizes were Saffman corrected (Saffman, 1987), and the drops were grouped in 100 size classes by a home-developed Matlab® procedure. For deducing global spray information, the local data were weighted with the local drop number flux and with the annular part of the spray cross section for which the data are representative (see the illustration in Fig. 4). The most important global spray property, the global Sauter mean drop size $D_{32,\mathrm{global}}$, is given by the equation

$$D_{32,\mathrm{global}} = \frac{\sum_{j=1}^{J}\sum_{i=1}^{I} D_i^3(r_j)\dot{n}(r_j,D_i)2\pi r_j \Delta r}{\sum_{j=1}^{J}\sum_{i=1}^{I} D_i^2(r_j)\dot{n}(r_j,D_i)2\pi r_j \Delta r} = \frac{\sum_{j=1}^{J}\sum_{i=1}^{I} D_i^3(r_j)\dot{n}(r_j,D_i) r_j}{\sum_{j=1}^{J}\sum_{i=1}^{I} D_i^2(r_j)\dot{n}(r_j,D_i) r_j}. \quad (1)$$

In this equation, $D_i(r_j)$ is the mean drop size of size class i at measuring point j, and $\dot{n}(r_j, D_i)$ denotes the number flux of the drops with sizes in size class D_i at the measurement position r_j, which was obtained by dividing the drop rate by the validation rate achieved in the PDA measurements. Validation rates of the order of 60% were reached, which is an indication for good measurements, given the partly high drop concentrations in the spray zones where the measurements were carried out. The term $2\pi r_j \Delta r$, which is the product of the mean circumference of the annular part j of the spray cross section and the width of the annulus, accounts for the position-dependent area of the annulus for which the local measurements are representative. The factor Δr was cancelled from the equation due to the equidistant arrangement of the measuring positions.

The above formulation of $D_{32,\mathrm{global}}$ implies the replacement of integrals over the drop size range and the spray cross section by sums of discrete rectangle areas – in the sense of a numerical integration by a quadrature formula. The error in this approximation depends on the radius of the cross section, the radial step width Δr, and the maximum variation of the functions $2\pi r\dot{n}(r, D)D^3$ and

Table 3
Data defining the 30 spray experiments – liquid properties, flow rate, pressure drop, and measured $D_{32,\mathrm{global}}$ and sheet opening angle α.

Experiment #	Atomizer configuration (–)	Dynamic viscosity μ (mPas)	Liquid density ρ (kg/m^3)	Surface tension σ (mN/m)	Mass flow rate $\dot{m}$ (kg/h)	Driving pressure difference Δp (bar)	Global Sauter mean diameter $D_{32,\mathrm{global}}$ (μm)	Sheet angle α (°)
1	SB – 30	16.26	1240	72	151	123	58.86	55
2	SB – 30	18.67	1247	72	173	152	52.92	50.5
3	SB – 70	12.13	1220	72	141	19	130.63	80
4	SD – 70	10.60	1213	72	187	22	113.06	72
5	SF – 30	14.24	1232	72	200	84	58.17	60
6	SF – 50	13.24	1226	72	234	38	92.62	55
7	SF – 70	8.69	1201	72	153	7.5	171.49	63
8	SB – 70	40.25	1276	72	152	22	112.61	61
9	SC – 70	48.66	1282	72	279	46	90.74	59
10	SD – 50	41.56	1277	72	312	71	72.74	50
11	SD – 70	52.85	1285	72	303	30	110.97	52
12	SF – 30	54.00	1288	72	200	80	66.46	15
13	SF – 50	32.50	1267	72	243	35	77.54	49
14	SF – 70	46.79	1281	72	351	29	100.02	47
15	SB – 70	127.83	1315	72	444	87	89.09	43
16	SC – 70	171.41	1310	72	423	89	73.60	42
17	SD – 50	140.00	1314	72	494	139	61.74	33
18	SD – 70	110.00	1306	72	388	46	91.62	45
19	SF – 50	116.16	1307	72	410	80	80.05	25
20	SF – 70	101.80	1304	72	538	58	80.91	42
21	SB – 30	63.45	1277	51.4	200	105	73.60	45
22	SB – 70	56.00	1269	48.5	211	30	103.58	54
23	SC – 70	57.84	1275	57.9	279	40	89.31	63
24	SD – 50	43.50	1257	52.0	312	73	63.88	64
25	SF – 50	65.57	1280	49.0	380	72	71.00	38
26	SF – 70	52.10	1250	52.1	391	39	79.01	56
27	SB – 70	166.90	1300	53.1	400	69	90.05	48
28	SC – 70	146.00	1290	49.7	400	54	91.43	47
29	SF – 70	157.60	1290	46.5	480	40	88.76	42
30	SC – 40	152.10	1297	51.5	250	65	88.04	23

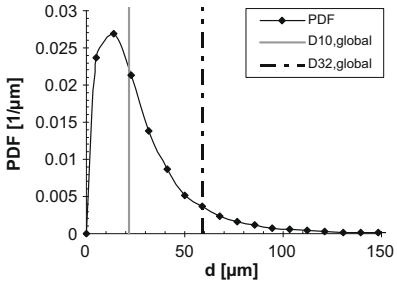

Fig. 5. Global Probability Density Function of the drop size and the global mean drop sizes from spray experiment #1 listed in Table 3.

$2\pi r\dot{n}(r,D)D^2$ with the radial coordinate. For experiment #23, the resulting maximum error is estimated in the order of 8% of $D_{32,global}$. In experiments with smaller spray angle, the accuracy is even better.

The drop size distribution of the entire spray is given by the global Probability Density Function (PDF). This function is given as

$$\mathrm{PDF}(D_i) = \frac{1}{\Delta D}\frac{\sum_{j=1}^{J}\dot{n}(r_j,D_i)r_j}{\sum_{j=1}^{J}\sum_{i=1}^{I}\dot{n}(r_j,D_i)r_j}, \tag{2}$$

where ΔD is the width of the 50 size classes used for computing the global size PDFs. The global drop size PDF of the spray from experiment #1, specified in Table 3, is depicted in Fig. 5 as an example. Next to the PDF, the global number mean and Sauter mean drop sizes, $D_{10,global}$ and $D_{32,global}$, are depicted in Fig. 5 by solid and dash-dotted lines, respectively.

2.3. The test liquids

The test liquids used were water–sucrose–ethanol solutions with varying composition. By changing the contents of the three mixture components, the liquid viscosity μ and the surface tension σ may be adjusted independently (Dorfner et al., 1995). The liquid density, however, cannot be controlled. The liquid properties were varied in the ranges $0.00869\ \mathrm{Pas} \leqslant \mu \leqslant 0.1714\ \mathrm{Pas}$, $0.0465\ \mathrm{N/m} \leqslant \sigma \leqslant 0.072\ \mathrm{N/m}$, and $1201\ \mathrm{kg/m^3} \leqslant \rho \leqslant 1315\ \mathrm{kg/m^3}$. The test liquids were characterized as follows: the dynamic viscosity was measured with capillary viscometers from Schott, types 501 20 and 501 23, since the liquids were all Newtonian in flow behavior. The surface tension against air was measured with a ring tensiometer Krüss K 8. Since the test liquids under investigation do not contain macromolecular, surface-active components, the equilibrium values of the surface tension obtained by these measurements occur in the atomization process also and are, therefore, relevant for the characterization. When measuring mixtures with an ethanol content, the measurements were carried out quickly to keep evaporation losses of the ethanol low. The density ρ of the liquids was measured with the flow meter sketched in Fig. 1, which was also used for measuring the liquid mass flow rate through the atomizer. The various physical properties of the test liquids, together with the physical conditions of the experiments and the atomizers used, are put together in Table 3. The global Sauter mean drop sizes $D_{32,global}$ and the cone angles α of the liquid sheets measured in the experiments are also listed in Table 3. The ambient medium in the spray experiments was always the air of the laboratory at a pressure of 1.013 bar and a temperature of $(20 \pm 1)^{\circ}\mathrm{C}$, resulting in an ambient air density of $1.204\ \mathrm{kg/m^3}$. This quantity, which has an influence on the spray formation due to the Kelvin–Helmholtz instability of the conical sheets, was not varied in the experiments and therefore does not appear as an influencing quantity in our study.

2.4. Measurement program

The experiments were planned using the method of the factorial experimental design. Basically, this design defines combinations of extreme values of the parameters to be chosen. In addition, intermediate states between the extremes may be included to enhance the information about influences from the various parameters on the process results. The parameters varied in the factorial design are the swirl chamber height, the orifice diameter, as well as the dynamic viscosity and the surface tension of the liquid. Mass flow rates were varied between 141 and 538 kg/h. Depending on the geometry of the atomizers and the liquid properties, such as the dynamic viscosity, this led to pressure drops across the atomizers between 7.5 and 152 bar. These spray conditions are relevant for the industrial production scale. Overall, 30 different spray experiments were carried out.

3. Characterization of the sprays resulting from sheet break-up

The results of the experiments essentially consist in the global Probability Density Function (PDF) of the spray drop size, and in moments or a ratio of moments of this PDF, such as the global number mean and Sauter mean drop sizes, $D_{10,global}$ and $D_{32,global}$. The PDA measurements, of course, provide much more detail, such as two velocity components of the drops and the times of arrival at and transit through the probe volume. The latter information, however, was not analyzed here, since the interest of the present investigation is focused on the spray drop size spectrum. Geometrical spray properties determined by image processing in this study were the sheet break-up length L and the opening angle α.

A dimensional analysis of the formation of the global Sauter mean drop size in the sprays was carried out. The list of parameters relevant for the drop formation includes the global Sauter mean drop size $D_{32,global}$ itself, the liquid density ρ, dynamic viscosity μ, and surface tension σ against air, the diameter d_{SC}, height h_{SC}, and inlet slit width b_{Ch} of the swirl chamber, the orifice diameter d_{Or}, and the driving pressure difference Δp.

The purpose of this analysis is to develop a universal representation of the global mean spray drop size $D_{32,global}$ as a function of the relevant influencing parameters. With the three basic dimensions m, s, and kg involved, the above set of nine parameters results in six independent non-dimensional groups characterizing the atomization result. The groups found by the analysis are the non-dimensional $D_{32,global}$, three length scale ratios representing the atomizer geometry, and the pressure-based Reynolds number as well as the Ohnesorge number of the process, which read

$$\left[\frac{D_{32,global}}{d_{SC}},\ \frac{d_{Or}}{d_{SC}},\ \frac{h_{SC}}{d_{SC}},\ \frac{b_{Ch}}{d_{SC}},\ \mathrm{Re}_p = \frac{\sqrt{\Delta p\rho}d_{SC}}{\mu},\ \mathrm{Oh} = \frac{\mu}{\sqrt{\sigma d_{Or}\rho}}\right].$$

Seeking a correlation for the non-dimensional $D_{32,global}$ in the form of a product of powers of the non-dimensional groups, times a constant, the exponents and the constant were determined by non-linear regression to the experimental data based on the least-squares method. The correlation found reads

$$\left(\frac{D_{32,global}}{d_{SC}}\right)_C = 3.074\ \mathrm{Re}_p^{-0.8505}\mathrm{Oh}^{-0.7538}\left(\frac{h_{SC}}{d_{SC}}\right)^{-0.0574}\left(\frac{d_{Or}}{d_{SC}}\right)^{-0.3496} \times \left(\frac{b_{Ch}}{d_{SC}}\right)^{-0.0426} \tag{3}$$

In Fig. 6, the values $(D_{32,global}/d_{SC})_C$ from correlation (3) are depicted together with the measured values from the 30 experiments given in Table 3. The correlation represents the experimental data with a coefficient of determination $R^2 = 0.9566$, which is an excellent result.

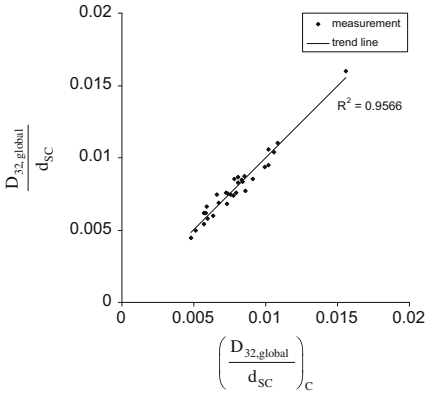

Fig. 6. Non-dimensional representation of the measured global Sauter mean drop size of the water–sucrose–ethanol solution sprays listed in Table 3 by correlation (3).

In the literature we find many correlations for mean drop sizes in sprays – not only from pressure-swirl atomizers (Lefebvre, 1989). In principle, all correlations for sprays from pressure-swirl atomizers resulting from a dimensional analysis should be of the form of Eq. (3), provided that the geometry of the atomizer may be represented by the length scale ratios given in that equation. One example is the correlation by Richter and Glaser (1987), which may be rewritten in terms of the presently defined quantities as

$$\left(\frac{D_{32,\mathrm{global}}}{d_{\mathrm{SC}}}\right)_{C,\mathrm{RG}} = C\mathrm{Re}_p^a \mathrm{Oh}^b \left(\frac{d_{\mathrm{Or}}}{d_{\mathrm{SC}}}\right)^c \left(\frac{b_{\mathrm{Ch}}}{d_{\mathrm{SC}}}\right)^d. \tag{4}$$

We see that, in contrast to our Eq. (3), the correlation (4) does not represent the influence of the swirl chamber height h_{SC}, which is due to the conical geometry of the downstream part of the atomizer swirl chamber investigated in that study. We can therefore expect this correlation to be less suitable for representing our data. Also, the agreement of this correlation with the data of the authors themselves is not as good as in our case (Richter and Glaser, 1987).

In the following, the sensitivity of the global Sauter mean drop size given by Eq. (3) against uncertainties in the measured quantities entering the right-hand side was analyzed. The geometric parameters of the nozzle may be measured with high accuracy and therefore bring in very low systematic errors. In contrast to this, the driving pressure difference and the liquid density and surface tension against air may be subject to stochastic errors due to the measuring techniques applied. Process parameters may furthermore be subject to fluctuations, which cannot be avoided. The total uncertainty of the global Sauter mean drop size as described by Eq. (3) can be written as

$$\frac{\Delta D_{32,\mathrm{global}}}{D_{32,\mathrm{global}}} = \sqrt{\left[-0.4253\frac{\Delta(\Delta p)}{\Delta p}\right]^2 + \left[0.3769\frac{\Delta\sigma}{\sigma}\right]^2 + \left[-0.0484\frac{\Delta\rho}{\rho}\right]^2 + \left[0.0967\frac{\Delta\mu}{\mu}\right]^2} \tag{5}$$

The relative uncertainties of the measured driving pressure difference $\Delta(\Delta p)/\Delta p$ and the surface tension are of the order of ±1%. The relative uncertainty of the measured liquid density $\Delta\rho/\rho$ is of the order of ±0.25%, as given by the producer of the Foxboro flow meter. The dynamic viscosity was measured with an uncertainty of ±1%. The total uncertainty of the measured global Sauter mean drop size $\Delta D_{32,\mathrm{global}}/D_{32,\mathrm{global}}$ then results from Eq. (5) as ±0.58%, which indicates a very high reproducibility of this quantity. The maximum deviation of an individual data point from correlation (3) is 11.6% of the measured value. Characterized by the coefficient of determination with the value of 0.9566, the correlation represents the experimental data very well. An additional parameter for characterizing the goodness of the fit is the coefficient of variation c_v, which is defined as

$$c_v = \frac{s(x)}{x_{\mathrm{mean}}} \tag{6}$$

Here, $s(x)$ denotes the sample standard deviation, and x_{mean} the sample mean value of a quantity x. In the present experiments, the coefficient of variation of the global Sauter mean drop size is calculated with the differences between measured and modeled values as the variable x. In view of the significance of the quantity c_v for the present study, the mean measured $D_{32,\mathrm{global}}$ is taken as the quantity x_{mean}. The coefficient c_v according to this definition for the data set in Fig. 6 has the value of 2.86%, which is an excellent result.

Another spray property of interest is a measure of the width of the global drop size PDF, i.e., the degree of variation of the drop size in the spray. For quantifying this, the root-mean square (standard deviation) of the drop size in the global spectra, $\mathrm{RMS}_{\mathrm{global}}(D)$, was determined. For plausibility reasons and from experimental evidence we can expect a relation between a global mean drop size and the $\mathrm{RMS}_{\mathrm{global}}$ to exist, which may represent an increase of the $\mathrm{RMS}_{\mathrm{global}}$ with the mean drop size. The local standard deviation of the drop size $\mathrm{RMS}(D)$ is defined as

$$\mathrm{RMS}(D) = \sqrt{\frac{1}{N-1}\sum_{i=1}^{I} n_i (D_i - D_{10})^2} \tag{7}$$

where N is the total number of drops in the ensemble, n_i the number of drops in size class i, and I the total number of size classes. The global standard deviation of the drop size $\mathrm{RMS}_{\mathrm{global}}(D)$ is calculated from the local PDA data as per

$$\mathrm{RMS}_{\mathrm{global}}(D) = \sqrt{\frac{\sum_{j=1}^{J}\sum_{i=1}^{I}\dot{n}(D_i,r_j)\cdot 2\pi r_j \Delta r (D_i - D_{10,\mathrm{global}})^2}{\sum_{j=1}^{J}\sum_{i=1}^{I}\dot{n}(D_i,r_j)\cdot 2\pi r_j \Delta r}} = \sqrt{D_{20,\mathrm{global}}^2 - D_{10,\mathrm{global}}^2} \tag{8}$$

(Sowa, 1992). The symbols $D_{10,\mathrm{global}}$ and $D_{20,\mathrm{global}}$ denote the global number mean and area-mean drop sizes, respectively. The size class summation extends over all global size classes i; the summation over all annular parts j of the spray cross section covers the whole cross section. By linear regression of the experimental data, the correlation

$$\mathrm{RMS}_{\mathrm{global}}(D) = 7.3504 + 0.1268 D_{32,\mathrm{global}} + 0.0008 D_{32,\mathrm{global}}^2 \tag{9}$$

was found, where the values of $D_{32,\mathrm{global}}$ must be entered in microns to yield the $\mathrm{RMS}_{\mathrm{global}}$ in microns. In Fig. 7, the correlation is depicted as a trend line to the experimental data in a diagram of the global standard deviation of the drop size as a function of the global Sauter mean drop size. The coefficient of determination has a value of 0.9757; the coefficient of variation is 3.28%, where the arithmetic mean of the measured values of the drop size RMS is the reference quantity x_{mean} of Eq. (6). It is seen that the global standard deviation of the drop size increases with the global Sauter mean drop size, which confirms the expectation. It is interesting to note that, according to relation (9), there exists a least scatter in the drop size in the sprays, even when the Sauter mean diameter becomes very

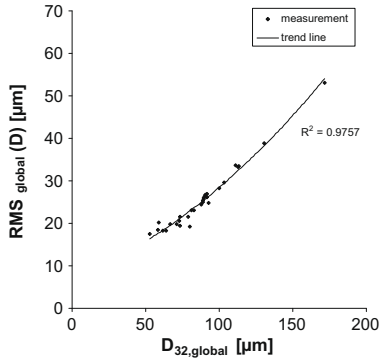

Fig. 7. Global standard deviation of the drop size as a function of the global Sauter mean drop size for the water–sucrose–ethanol solution sprays listed in Table 3.

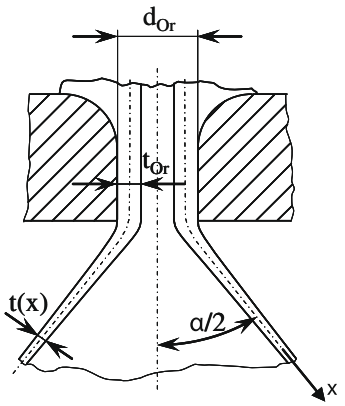

Fig. 8. Sketch of the liquid flow through the atomizer orifice and the conical sheet with its cone angle α and thickness $t(x)$.

small. This relation seems to exist between the dimensional quantities; it is unnecessary to non-dimensionalize the data, despite the strong variations of liquid properties, atomizer geometry, and operation conditions. A further investigation of this finding is beyond the scope of the present paper.

Having carried out this experimental survey of spray formation with pressure-swirl atomizers, in the following sections a theoretical basis is presented for establishing a relation of the relevant parameters of the spraying process not only with moments of the drop size spectra, but also with the shape of the spectra.

4. Prediction of the atomization result by the Dombrowski and Johns model

The basis of the prediction of the atomization result by the approach of Dombrowski and Johns (1963), which is widely accepted in the literature, is a stability analysis of the liquid sheet and of the ligaments formed by the sheet break-up. For this analysis it is important to know the sheet velocity and thickness in the break-up zone, and the physical properties of the liquid and the ambient gaseous medium. For determining the sheet velocity and thickness, various methods are established in the literature (e.g., Lefebvre, 1989; Dahl and Muschelknautz, 1992; Walzel, 1998; Senecal et al., 1999; Schmidt et al., 1999). The results presented here are based on Walzel (1998) and Schmidt et al. (1999), who define a velocity number φ as the ratio of the liquid sheet velocity U to the potential velocity:

$$\varphi = \frac{U}{\sqrt{2\,\Delta p/\rho}} \tag{10}$$

For given mass flow rate $\dot{m}$, driving pressure difference Δp, sheet opening angle α, and geometry of the atomizer, the smallest possible velocity number $\varphi_{\min}$ occurs when the air core in the pressure-swirl atomizer disappears, so that the liquid fills the whole orifice cross section. This value of the velocity number is given as

$$\varphi_{\min} = \frac{4\dot{m}[\pi\rho d_{Or}^2\cos(\alpha/2)]}{\sqrt{2\Delta p/\rho}} \tag{11}$$

(Schmidt et al., 1999). The largest possible velocity number $\varphi_{\max}$ arises when the pressure energy is converted into kinetic energy without losses, i.e., when the liquid sheet velocity is the potential velocity. Then φ exhibits the value $\varphi_{\max} = 1$. As an alternative for the velocity number φ, Lefebvre (1989) specifies a correlation for the discharge coefficient c_D, which turns out problematic for the present work, since in some cases it predicts values of c_D greater than 1, which is unphysical. Schmidt et al. (1999) use an expression which turns out inappropriate for the present work, since it predicts that the air core in the atomizer disappears in a number of experiments of the present study, where this was not the case.

As an alternative approach to get a good estimate of the velocity number φ, we take the arithmetic mean of the two extremes of φ, i.e., we set

$$\varphi = \frac{1}{2}(\varphi_{\max} + \varphi_{\min}) = \frac{1}{2}(1 + \varphi_{\min}) \tag{12}$$

This relation represents the present experiments best, which was found from comparisons of the sheet velocity following from Eqs. (10)–(12) above with the velocities of very large drops in the sprays measured with the PDA close to the sheet break-up zone.

From the velocity number φ, then, the sheet velocity U is calculated. Next, for calculating the sheet thickness, we assume a conical sheet with constant cross section normal to the direction of the sheet velocity. This configuration is sketched in Fig. 8. The sheet thickness then comes out proportional to the inverse of the distance from the pole of the flow. Denoting the radial extension of the sheet (normal to the symmetry axis of the atomizer) r, and the state at the orifice with subscript Or, the thickness of the annular film t_{Or} there is obtained from a formulation of the constant liquid volume flow rate as

$$t_{Or} = \frac{d_{Or}}{2}\left(1 - \sqrt{1 - \frac{4\dot{m}/\rho}{\pi d_{Or}^2 U\cos(\alpha/2)}}\right) \tag{13}$$

The constant sheet cross section and velocity lead to the formulation of the sheet thickness at a sufficient distance from the orifice

$$t(x) = \frac{\dot{m}/\rho}{\pi U[d_{Or} - t_{Or} + 2x\sin(\alpha/2)]} \tag{14}$$

In Eq. (14), the x-coordinate is oriented in the direction of the sheet motion, as sketched in Fig. 8. The origin $x = 0$ is located at the orifice. The sheet thickness t is measured normal to the direction of the sheet velocity U. Its value in the break-up zone is important for determining the ligament diameter, and, consequently, the drop size.

In a next step, the mechanism of drop formation in sprays based on the growth of unstable waves on the surface of the sheets is discussed. This analysis is needed since, on the one hand, it is attempted to reproduce the measured mean spray drop sizes by applying the drop formation mechanism proposed by Dombrowski and Johns (1963). On the other hand, the liquid sheet parameters relevant for its disintegration, which are essential also for modeling the measured drop size spectra in a later step, follow from this analysis. One essential pair of parameters are the wavelength and growth rate of the fastest growing unstable wave on the sheet.

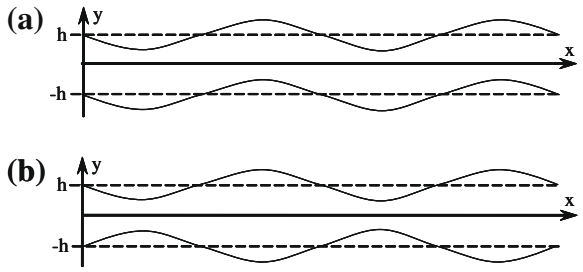

Fig. 9. Disturbance waves on plane liquid sheets: (a) antisymmetric or sinuous waves and (b) symmetric or varicose waves (adapted from Senecal et al., 1999).

Stability analyses of liquid sheets formed in atomization processes with pre-filming atomizers were carried out by a number of researchers, e.g., Squire (1953), Dombrowski and Johns (1963), Li and Tankin (1991), and Senecal et al. (1999). Dombrowski and Johns considered the Kelvin–Helmholtz instability of liquid sheets under the influence of surface tension and liquid viscosity. They derived a dispersion relation for the growth rate of long waves, using a one-dimensional model of the liquid sheet. However, neglecting variations of the shear stress across the thickness of the liquid sheet, the determined dispersion relation turned out incorrect for viscous liquid sheets, since it cannot represent the continuity of the shear stress across the interface (Senecal et al., 1999). Li and Tankin (1991) considered these variations, but assumed dominant growth of long-wave disturbances, which leads to inaccuracies in the prediction of sheet instability for conditions found with many pre-filming atomizers. Senecal et al. (1999) pointed out that the liquid sheet disintegration, characterized by values of the gas Weber number

$$We_g = \frac{\rho_g U^2 t_{\mathrm{Or}}}{2\sigma} \tag{15}$$

exceeding the threshold of 1.69, is dominated by short-wave disturbances. In the gas Weber number, ρ_g denotes the gas density and σ the surface tension of the liquid against the ambient gas.

In the present study we investigate two-dimensional viscous incompressible liquid sheets of thickness $t = 2$ h, as described by Li and Tankin (1991), as well as by Senecal et al. (1999). The sheet moves in x-direction through a gaseous medium which is assumed to be quiescent, inviscid, and incompressible. The orientations of the coordinate axes are depicted in Fig. 9. Disturbances of the liquid sheet, e.g., deformations η of its surfaces, are described in the exponential form

$$\eta = \Re[\eta_0 \exp(ikx + \omega t)] \tag{16}$$

Here, η_0 is the initial wave amplitude, $k = 2\pi/\lambda$ is the (real) wave number, and ω is the complex frequency. Therefore, the stability analysis carried out is temporal. The disturbance responsible for the sheet break-up is the one with a wave number K_s leading to the largest growth rate Ω_s. The wavelength of this disturbance, together with the sheet thickness at break-up, determines the resulting ligament diameter. This most unstable disturbance is found from the dispersion relation $\omega = f(k)$ of the moving sheet. This dispersion relation represents the jump condition of the normal stress across the deformed liquid–gas interface as a result of capillary pressure in the sheet due to the deformation.

The liquid normal stress at the interface follows from the solution of the equations of continuity and momentum of the liquid sheet flow, formulated in the disturbance quantities. Decomposing the velocities and pressure into an irrotational and a rotational part, the linearized equations of continuity and momentum can be expressed in terms of a velocity potential ϕ and a stream function ψ. Hence, the normal stress in the liquid sheet can be formulated in terms of the velocity potential based momentum equation (Li and Tankin, 1991). The gas normal stress at the interface is determined by the continuity and momentum equations for the gas, which is assumed to be inviscid and at rest in its undisturbed state. The pressure induced by surface tension on the deformed interfaces is related to the curvature of the interface.

The normal stresses in the liquid and the gaseous phases, and the pressure induced by surface tension, are mutually related by the liquid sheet dynamic boundary condition for the normal stress at the interface, which yields the following dispersion relation between the complex frequency ω and the disturbance wave number k for antisymmetric disturbances:

$$\left[\rho(\omega + ikU) + 2\mu k^2\right]\left[\frac{\mu}{\rho}(k^2 + s^2)\right]\tanh(kh) - 4\frac{\mu^2}{\rho}k^3 s\tanh(sh) + \rho_g\omega^2 + \sigma k^3 = 0 \tag{17}$$

(Li and Tankin, 1991). The corresponding relation for symmetric disturbances is very similar to (17), with $\tanh(kh)$ and $\tanh(sh)$ replaced by $\coth(kh)$ and $\coth(sh)$, respectively. Liquid sheets with antisymmetric and symmetric deformations are depicted in Fig. 9. In both cases, s represents the parameter

$$s = \sqrt{k^2 + \rho(\omega + ikU)/\mu} \tag{18}$$

An order of magnitude analysis shows that the terms of second order in viscosity in (17) can be neglected against the other terms (Senecal et al., 1999). With this simplification, and by rearrangement, the growth rate for the antisymmetric disturbances is given by

$$\omega_r = -\frac{2\mu k^2\tanh(kh)}{\rho[\tanh(kh) + Q]} + \frac{\sqrt{4\mu^2k^4\tanh^2(kh)/\rho^2 - Q^2U^2k^2 - [\tanh(kh) + Q](-QU^2k^2 + \sigma k^3/\rho)}}{\tanh(kh) + Q} \tag{19}$$

(Senecal et al., 1999). Here, ω_r denotes the real part of the complex frequency, which is the rate of growth of the disturbances, and Q is the ratio of the gas to liquid densities, ρ_g/ρ, which is $O(10^{-3})$.

Senecal et al. (1999) point out that sheets under the influence of Kelvin–Helmholtz instability in a gaseous environment are subject to short wave-dominated atomization, if the gas Weber number exceeds the value of 1.69. Consequently, the dominant wave numbers are large, and the values of the functions $\tanh(kh)$ and $\coth(kh)$ converge to unity. If additionally the smallness of the density ratio $Q \ll 1$ is accounted for, Eq. (19) reduces to

$$\omega_r = -\frac{2\mu k^2}{\rho} + \sqrt{\frac{4\mu^2k^4}{\rho^2} + QU^2k^2 - \frac{\sigma k^3}{\rho}} \tag{20}$$

which is also obtained for the symmetric mode. By requiring the derivative of ω_r with respect to k to vanish at the maximum of the function, the wave number K_s (and the related wavelength Λ_s) corresponding to the maximum growth rate Ω_s is obtained. The equation determining K_s is of third order and must be solved numerically.

Based on these disturbance parameters, the sheet disintegration process can be quantified following the mechanism proposed by Dombrowski and Johns (1963). Since the growth rate of short waves does not depend on the sheet thickness, as seen in Eq. (20), the sheet break-up length L is calculated as follows:

$$L = U\tau = \frac{U}{\Omega_s}\ln\left(\frac{\eta_b}{\eta_0}\right) \tag{21}$$

Here, U denotes the sheet velocity, which is at the same time the relative velocity between the liquid and the quiescent gas. τ denotes the break-up time, and η_b is the value of the sheet deformation at break-up. The quantity $\ln(\eta_b/\eta_0)$ has the value of 12 (Senecal et al., 1999). The break-up length L plays the role of the x-coordinate in Eq. (14) and determines the sheet thickness $t_b = t(L)$ at break-up, which, together with the wavelength of the dominant disturbance, defines the cross-sectional area of the ligaments detached from the sheet. The diameter of the ligaments d_L separated from the liquid sheet in the break-up zone is found from a volume balance as

$$d_L = \sqrt{\frac{8t_b}{K_s}} \tag{22}$$

In this balance it is assumed that ligaments are formed from tears in the sheet once per wavelength, which is typical for short wave atomization (Senecal et al., 1999).

The last step of the spray formation process is the break-up of the ligaments into drops. The diameter of the drops d_D formed by this process may be calculated using Weber's result for the wavelength of the fastest growing disturbance on a cylindrical viscous liquid jet, which leads to the equation

$$d_D = 1.88 d_L(1 + 3\mathrm{Oh})^{1/6} \tag{23}$$

for the drop size (Weber, 1931). Here, Oh denotes the Ohnesorge number

$$\mathrm{Oh} = \frac{\mu}{\sqrt{\rho\sigma d_L}} \tag{24}$$

The calculation of the drop size based on these assumptions leads to an unsatisfactory result, which is shown by the comparison with the measured global Sauter mean drop sizes $D_{32,\mathrm{global}}$ (Dombrowski and Johns, 1963) depicted in Fig. 10. The inaccuracy is quantified by the coefficient of variation c_v – with the arithmetic mean value of the measured global Sauter mean drop sizes as the reference quantity x_{mean} – of 27.2%, which represents large deviations of the model data from the measured values. This finding is in agreement with the data in Dombrowski and Johns (1963), which also show unsatisfactory agreement between the measured and the calculated drop sizes, although with less scatter than presently seen. Problematic is also that the model predicts very large sheet break-up lengths in a number of cases, which is in conflict with the break-up lengths measured by photographic visualization in our study, as presented in Table 4. These discrepancies clearly indicate the need for an alternative approach.

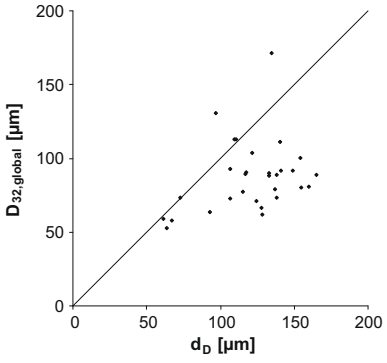

Fig. 10. Comparison of the measured global Sauter mean drop size $D_{32,\mathrm{global}}$ and the drop size d_D calculated by the Dombrowski and Johns model. The underlying experiments are listed in Table 3.

5. Prediction of drop size spectra in the sprays

An alternative to the above described method of predicting mean diameters of the droplets in the sprays is to predict the global drop size spectrum, from which the mean diameters can then be deduced. This approach avoids the calculation of the drop size invoking the Dombrowski and Johns model and the hypothesis that the ligaments formed in the sheet disintegration break up into droplets through the capillary mechanism described by Weber (1931).

The drop size spectrum in a spray is represented by a Probability Density Function. This function is obtained experimentally by measurements with phase-Doppler anemometry (PDA). The function is represented in a discrete form by measurement data grouped in size classes. The aim of the prediction of this function is to find a model function suitable for representing the spectrum most accurately with a minimum number of free parameters. The suitability of the model function is judged by comparison of the function with the measured data, and also of moments of the function with moments measured, such as the number mean and Sauter mean drop sizes. The model function searched for should be derived from physical principles. One approach is to apply the maximum-entropy formalism. The requirement that the Shannon entropy of the spray should be a maximum leads to the following three-parameter generalized gamma distribution characterizing the spray drop size spectrum (Dumouchel, 2006):

$$\mathrm{PDF}(d) = \frac{v^v}{\Gamma(v)} q \frac{d^{qv-1}}{d_{q0}^{qv}} \exp\left(-v\left(\frac{d}{d_{q0}}\right)^q\right) \tag{25}$$

In this function, which is a Probability Density Function, d is the drop size, v and q denote non-dimensional parameters, and d_{q0} is a constraint drop size.

An alternative to obtain a suitable mathematical representation of the drop size PDF is to consider the formation of spray drops by the break-up of ligaments, as in the present case. The form of the drop size distribution can then be determined by the model suggested by Villermaux et al. (2004). In their model, the spray drops are formed by an aggregation process of sub-drops that make up the ligaments. According to this model, the sub-drops are arranged in several sub-layers of the ligaments, as sketched in Fig. 11. In this process, the spray drop size is larger than the thickness of the ligaments, since the drops result from sub-drop coalescence. This model feature corresponds to experimental evidence. The time-dependent distribution of the sub-drop sizes is directed by the coalescence of the interacting sub-drops in the adjacent sub-layers. Under the assumption of uncorrelated sizes of the interacting sub-drops, the development of the sub-drop size distribution is directed by a convolution of the independent sub-drop size distributions. Since the sub-layers are assumed to be mutually independent, the distribution of the final spray drop size is also directed by a convolution. The solution of the corresponding evolution equation is the number-based drop size probability p_B,

Table 4
Properties of the 30 spray experiments relevant for the liquid sheet instability. The gas Weber number is calculated with $\rho_g = 1.204$ kg/m^3.

Experiment #	Liquid sheet velocity U (m/s)	Wavelength of the dominant disturbance Λ_s (μm)	Measured break-up length L_{meas} (mm)	Predicted break-up length L_{pred} (mm)	Gas Weber number We_g (–)
1	112.2	84.36	10	12.30	19.87
2	124.8	75.10	10	11.52	24.74
3	36.3	539.52	11	63.85	2.63
4	40.8	426.98	9	50.31	3.82
5	115.5	76.74	10	10.94	37.98
6	62.9	208.05	13	26.55	10.49
7	26.0	951.09	17	106.24	2.02
8	37.1	713.87	22	101.49	2.42
9	56.3	392.15	18	62.91	6.85
10	82.3	202.96	15	34.14	16.87
11	48.8	508.39	24	80.59	6.53
12	103.4	162.30	18	30.82	24.58
13	60.3	299.35	21	44.62	9.97
14	50.4	460.70	31	71.57	7.92
15	77.8	386.91	33	86.24	13.88
16	77.6	458.05	33	110.61	13.07
17	115.7	230.64	24	59.00	35.05
18	60.0	524.05	30	104.38	9.82
19	90.6	295.18	23	66.67	23.03
20	71.9	385.12	30	78.78	16.95
21	115.8	128.21	11	28.54	40.15
22	44.8	480.03	21	82.16	5.97
23	54.0	402.50	17	69.68	8.50
24	86.0	164.32	12.5	30.34	26.98
25	87.5	191.83	23	40.47	32.15
26	59.3	315.17	23	55.39	15.32
27	70.4	456.95	37	115.87	15.89
28	64.7	464.93	30	112.53	16.02
29	61.7	505.23	30	125.69	20.74
30	83.8	334.05	16	87.44	23.25

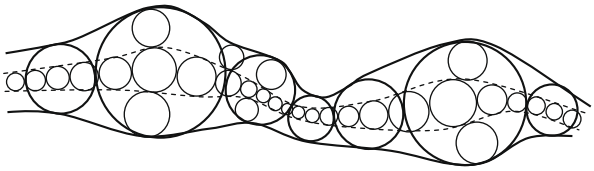

Fig. 11. Illustration of a ligament consisting of sub-drops in three sub-layers (adapted from Villermaux, 2007).

which is similar to (25) and is given in non-dimensional form as (Villermaux et al., 2004).

$$p_B(x) = \frac{v^v}{\Gamma(v)} x^{v-1} \exp(-vx) \tag{26}$$

Here, x denotes the non-dimensional spray drop size d/d_L, with the dimensional spray drop size d and the ligament diameter d_L, and the gamma distribution parameter v. The function satisfies the normalization condition.

$$\int_0^\infty p_B dx = 1 \tag{27}$$

The coalescence process leads to a drop size distribution characterized by an exponential decrease in the range of large drops (Villermaux, 2007). Consequently, also the drop size distribution of the resulting spray exhibits this characteristic. This feature is represented correctly by the gamma distribution (26).

A disadvantage of the formulation of the gamma distribution p_B in Eq. (26) can be seen in the role of the ligament diameter d_L. The formation of ligaments is believed to be due to the detachment of liquid portions from the end of the liquid sheets deformed by surface waves, as discussed in Section 4. Both the sheet break-up length and the ligament diameter deduced from this analysis are subject to uncertainties, as pointed out in Section 4. It is therefore desirable to avoid the ligament diameter as a reference length scale.

As an alternative, an empirical gamma distribution $p_{B,E}$ is specified as dependent on a modified non-dimensional spray drop size x, containing the wavelength of the dominant disturbance Λ_s and a parameter κ. The wavelength Λ_s, as calculated in Section 4, is presented in Table 4 for the 30 experiments of this study and can be regarded as a reliable sheet property. The parameter κ is introduced as a scaling parameter (Villermaux et al., 2004). Thus, the gamma distribution $p_{B,E}$ is written by modification of Eq. (26) as

$$p_{B,E} = \frac{v^v}{\Gamma(v)} \left(\frac{d}{\Lambda_s \kappa}\right)^{v-1} \exp\left(-v\frac{d}{\Lambda_s \kappa}\right) \tag{28}$$

The dimensional form of the gamma distribution $p_{B,E}$ in Eq. (28) is obtained by dividing the gamma distribution by the wavelength Λ_s and the parameter κ. The so obtained number-based drop size PDF reads

$$\mathrm{PDF}(d) = \frac{1}{\Lambda_s \kappa} \frac{v^v}{\Gamma(v)} \left(\frac{d}{\Lambda_s \kappa}\right)^{v-1} \exp\left(-v\frac{d}{\Lambda_s \kappa}\right) \tag{29}$$

This gamma distribution also satisfies a normalization condition. A typical gamma-distribution-based drop size spectrum is depicted in Fig. 12 together with the experimental data from spray experiment #23 defined in Table 3. The values of the parameters of the gamma distribution were found by fitting the function to the experimental data using the least-squares method. The value of Λ_s is determined by the conditions of experiment #23. The coefficient of determination R^2 has the value of 0.9918, which indicates an excellent representation of the measured data.

At first appearance in Fig. 12a, the representation of the whole measured drop size spectrum by the modeled PDF is excellent, although, for small drop sizes up to 20 μm, the model seems to slightly over-predict the measured data, and for drop sizes above 50 μm the measured data are slightly under-predicted. For a model function with only two independent parameters (v and κ), however,

the achieved agreement is excellent. Nonetheless, the representation of this set of data with logarithmic scaling of the ordinate axis in Fig. 12b shows deviations in the range of the large drop sizes. Although the values of the PDF in this range are small, these deviations lead to considerable differences between measured and modeled higher-order moments of the spectra as, e.g., in the global Sauter mean drop size $D_{32,\mathrm{global}}$. This is due to the fact that this mean diameter depends on the cubed and squared drop size. Since large drops contribute strongly to the overall liquid volume and surface area of the spray, even small numbers of large drops influence the Sauter mean diameter strongly. This is confirmed by the comparison of the global number mean and Sauter mean drop sizes, $D_{10,\mathrm{global}}$ and $D_{32,\mathrm{global}}$, as derived from the measured PDA data and as modeled with the gamma-distribution-based Probability Density Function (29), shown in Fig. 13. While the comparison of the global number mean drop size $D_{10,\mathrm{global}}$ in Fig. 13a shows reasonable agreement between measurement and prediction by the model, there is a substantial under-prediction of the global Sauter mean drop size $D_{32,\mathrm{global}}$, shown in Fig. 13b. This is quantified by the coefficients of variation of the data set, which have the values of 6.5% for $D_{10,\mathrm{global}}$, and 12.6% for $D_{32,\mathrm{global}}$. The reference quantities are the respective mean values of the measured global mean drop sizes from all the 30 experiments. Consequently, the present gamma distribution model as given by Eq. (29) turns out unsuitable for predicting higher-order moments of the drop size spectra.

This finding indicates that, for a more accurate prediction of higher-order moments of the drop size spectrum, the probability density of large drop sizes must be represented better than by the function (29). This improvement can be achieved by an appropriate modification of the gamma distribution. This was done empirically by adding an exponential term to the function, which raises the large drop size probability density, but changes the probabilities of the small sizes only slightly. The resulting modified Probability Density Function $\mathrm{PDF}_{\mathrm{Mod}}$ reads

$$\mathrm{PDF}_{\mathrm{Mod}}(d) = \frac{1}{(1+C_1C_2^2)}\left[\frac{1}{\Lambda_s\kappa}\frac{v^v}{\Gamma(v)}\left(\frac{d}{\Lambda_s\kappa}\right)^{v-1}\exp\left(-v\frac{d}{\Lambda_s\kappa}\right) + C_1\frac{d}{\Lambda_s^2}\exp\left(-\frac{d}{\Lambda_s C_2}\right)\right] \tag{30}$$

In this equation, the additional exponential term contains the drop size d, the wavelength of the dominant disturbance Λ_s, and two additional non-dimensional parameters C_1 and C_2. The factor in front of the square brackets follows from the normalization condition for the modified Probability Density Function. As a consequence of this modification, the function has the four adjustable

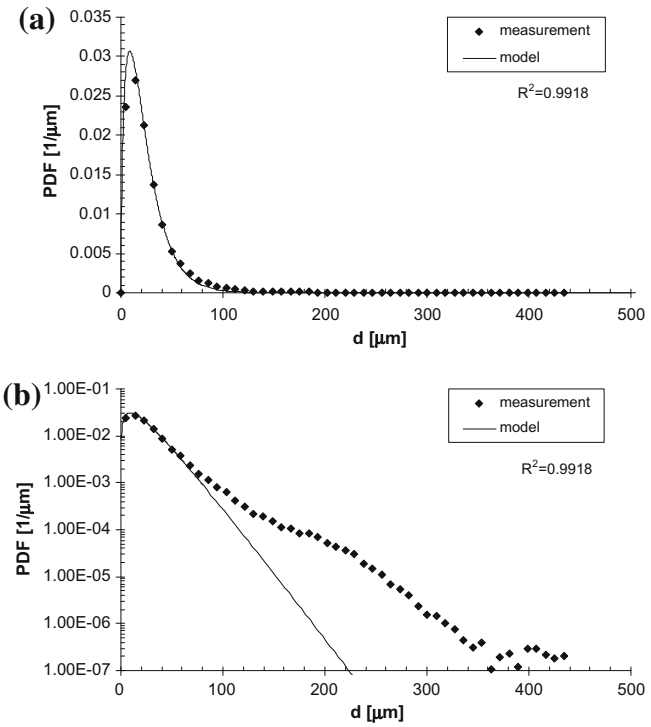

Fig. 12. (a) Measured and gamma distribution-modeled global Probability Density Functions of the drop size from spray experiment #23 and (b) the same data in a semi-logarithmic representation.

parameters v, κ, C_1, and C_2. It is well known that an increase of the number of parameters improves the goodness of fits to experimental data. However, the mathematical form of the function is also important for getting a physically plausible representation of the experiment. It is believed that this requirement is met by the present modified function better than with many functions studied in earlier publications (e.g., Bhatia and Durst, 1989; Xu et al., 1993; Paloposki, 1994).

The drop size spectrum defined by Eq. (30) was computed to represent the experimental data of spray experiment #23 specified in Table 3. The data of this experiment were presented in Fig. 12 above already in comparison with the model function given by Eq. (29). For computing the modified function, the gamma distribution parameter v and the parameter κ were taken from the function (29); only the parameters C_1 and C_2 were newly

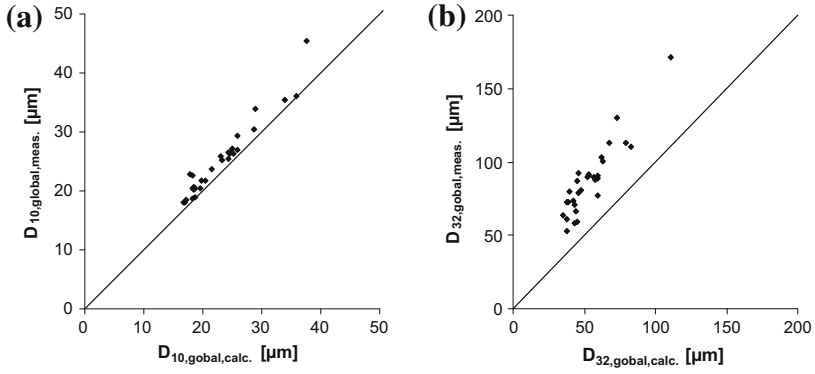

Fig. 13. Comparison of (a) the global number mean drop size $D_{10,\mathrm{global}}$ and (b) the global Sauter mean drop size $D_{32,\mathrm{global}}$ from the measurements and from the gamma distribution-based Probability Density Function (29) for the experiments in Tables 3 and 5. The individual values of the parameters v and κ of the gamma distribution were obtained by fits to the corresponding experimental data.

determined using the least-squares method for best fit to the measured global drop size PDF (an attempt to re-determine the whole set of parameters revealed less agreement). The results are shown in Fig. 14, where the solid lines indicate the Probability Density Function (30), and the dashed lines characterize the contribution of the exponential term added to the original gamma distribution from Eq. (29). These data show far better agreement between the modeled and measured spectra, both in the linear and in the semi-logarithmic representations, than seen in Fig. 12. This is confirmed by the slight increase of the coefficient of determination R^2 to a value of 0.9943. As an effect of the modification, further to the fairly good match of the spectra in the range of large drop sizes, the over-representation of small drops seen in Fig. 12a is also reduced. To support the present approach, Figs. 15 and 16 show the data from experiments #1 and #2.

Similar to Fig. 13, a comparison of the global number mean and Sauter mean drop sizes, $D_{10,\mathrm{global}}$ and $D_{32,\mathrm{global}}$, as obtained from measurements and modeled with the modified gamma distribution (30), is shown in Fig. 17. Here, especially the significant improvement of the overall agreement between the measured and the calculated global Sauter mean drop sizes over the data in Figs. 10 and 13b is noteworthy. The calculated global number mean drop sizes are also in better agreement with the measurements. The coefficient of variation of the data set of the global number mean drop size $D_{10,\mathrm{global}}$ is 3.6%, and for the global Sauter mean drop size $D_{32,\mathrm{global}}$ it is 4.8%. Thus, an accurate prediction even of higher-order moments of the drop size spectra is achieved with the modified gamma-distribution-based Probability Density Function $\mathrm{PDF_{Mod}}$ found in this study. For the comparisons in Fig. 17, the values of the four parameters of the function (30) were computed individually for each of the 30 experiments. These values, however, cannot be determined a priori for a given experiment. It is therefore of big interest to relate the values of the parameters to characteristic data of each experiment, which are easily accessible.

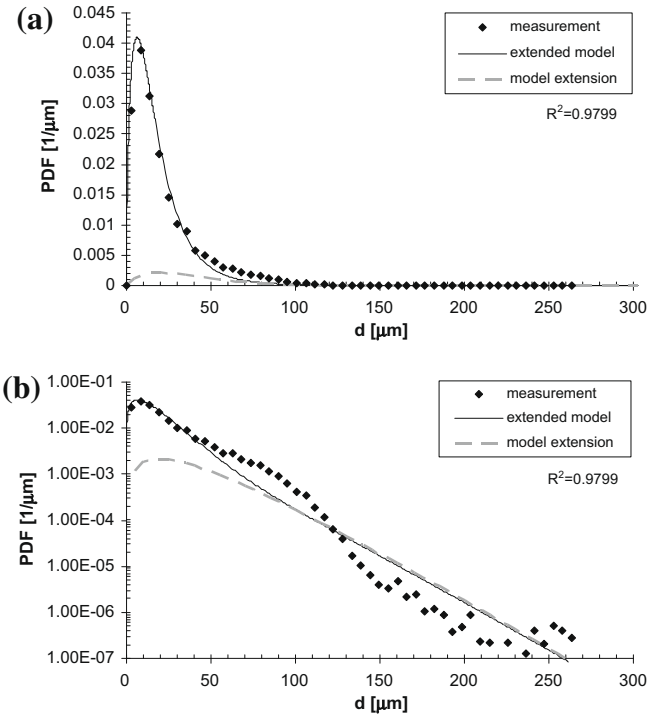

Fig. 15. (a) Measured and extended gamma distribution-modeled global Probability Density Functions of the drop size from spray experiment #1 and (b) the same data in a semi-logarithmic representation.

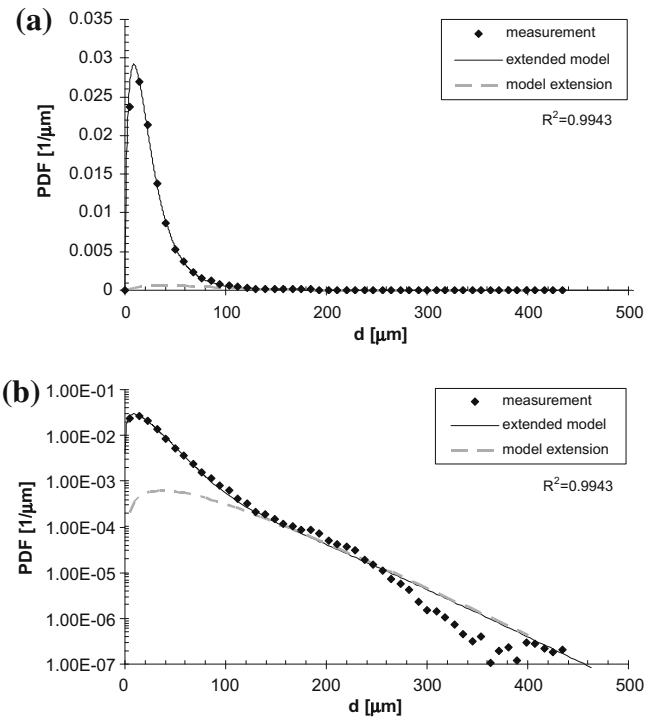

Fig. 14. (a) Measured and extended gamma distribution-modeled global Probability Density Functions of the drop size from spray experiment #23 and (b) the same data in a semi-logarithmic representation.

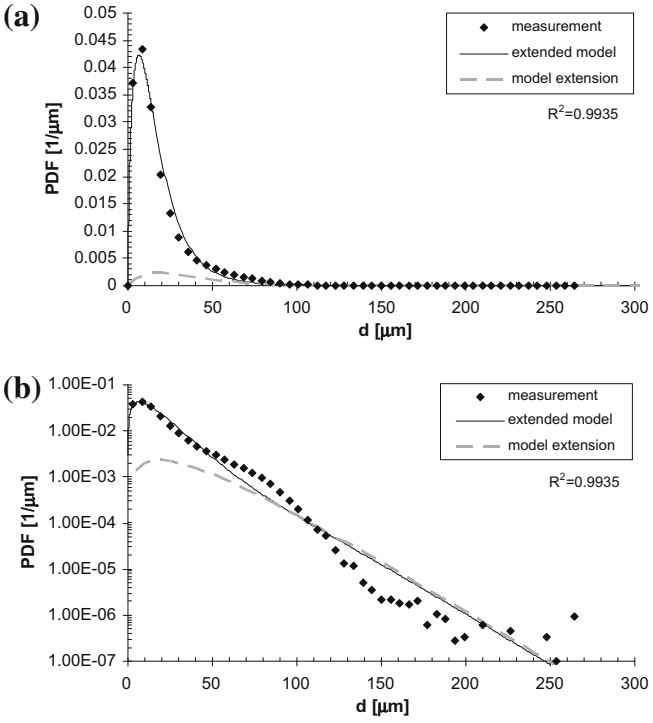

Fig. 16. (a) Measured and extended gamma distribution-modeled global Probability Density Functions of the drop size from spray experiment #2 and (b) the same data in a semi-logarithmic representation.

Therefore, in a further step, the four parameters of function (30) were modeled in a universal manner. The gamma distribution parameter ν was modeled as a function of the ratio of the orifice diameter of the atomizer to the liquid sheet thickness at the orifice, d_{Or}/t_{Or}, and the gas Weber number We_g. It was found that ν can be expressed as a product of powers of these two parameters, where the constant and the exponents were determined by non-linear regression analysis of the experimental data. The correlation found for the gamma distribution parameter ν reads

$$\nu = 0.4867 We_g^{0.2068} \left(\frac{d_{Or}}{t_{Or}}\right)^{0.4040} \tag{31}$$

The parameters κ, C_1, and C_2 were modeled as functions of the non-dimensional wavelength Λ_s/d_{sc} of the dominant disturbance. Once again, the constants and the exponents were obtained from a non-linear regression analysis of the 30 experiments with the test liquid sprays. The three correlations read.

$$\kappa = 0.00549 \left(\frac{\Lambda_s}{d_{SC}}\right)^{-0.7211} \tag{32}$$

$$C_1 = 79.299 \left(\frac{\Lambda_s}{d_{SC}}\right)^{0.7274} \tag{33}$$

$$C_2 = 0.0160 \left(\frac{\Lambda_s}{d_{SC}}\right)^{-0.5362} \tag{34}$$

The individual data of these four distribution parameters, together with their representation by the correlations, can be seen in Fig. 18 for each experiment. While the gamma distribution parameter ν is represented by this model with limited accuracy, as indicated by the coefficient of determination with a value of only 0.6464, the representation of the other three parameters by the correlations is supported by the high values of the coefficient of determination R^2 of 0.9216 for κ, 0.8177 for C_1, and 0.9128 for C_2.

In Table 5, the values of the four parameters are given together with the global number mean and Sauter mean drop sizes, $D_{10,global}$ and $D_{32,global}$, measured in the experiments. The values of the four parameters were found by individual fits to the experimental data.

As a concluding investigation, the global number mean and Sauter mean drop sizes of the sprays, $D_{10,global}$ and $D_{32,global}$, were determined by the modified gamma-distribution-based Probability Density Function PDF_{Mod}, applying the distribution parameters as calculated from the respective correlations (31)–(34). A comparison of the global number mean drop size $D_{10,global}$ and the global Sauter mean drop size $D_{32,global}$, as derived from the PDA data and modeled with the extended gamma-distribution-based Probability Density Function, is depicted in Fig. 19, respectively. As can be seen in these figures, there is good overall agreement between the measured and the modeled mean drop sizes, which is, however, less than with the individually determined parameters as presented in Fig. 17. This is indicated by the increase of the coefficient of variation from the value of 3.6% in Fig. 17a to 10% in Fig. 19a for the global number mean drop size, and from the value of 4.8% in Fig. 17b to 9.8% in Fig. 19b for the global Sauter mean drop size. An exception is the result of experiment #7, which exhibits the biggest measured $D_{10,global}$ and $D_{32,global}$, representing at the same time the largest deviations from the model, which are 25.8% for the global number mean drop size $D_{10,global}$, and 22.5% for the global Sauter mean drop size $D_{32,global}$, each value with the respective measured value as the reference quantity. The reason for this deviation can be found in the spray conditions of this experiment, which are characterized by a gas Weber number of 2.02, as given in Table 4. Since short wave-dominated atomization, which is presumed in all present experiments, presupposes gas Weber numbers well above 1.69, the closeness of $We_g = 2.02$ to this threshold in experiment #7 indicates the importance of considering also long-wave disturbances in this particular experiment. Thus, the determination of spray properties for this experiment based on short-wave disturbances may be the reason for the inaccurate representation of this result by the model.

In general, the good agreement between measured and calculated mean drop sizes supports the high value of the developed model function for representing drop size spectra in hollow-cone sprays from pressure-swirl atomizers of the present type.

6. Conclusions

Sprays from Newtonian liquids produced by pressure-swirl atomizers of the Delavan type SDX were characterized experimentally for their drop size spectra and global mean drop sizes. For measuring drop sizes, phase-Doppler anemometry was used. The measured global Sauter mean drop sizes were represented by a universal correlation obtained by dimensional analysis. The correlation is reproducible with an uncertainty of ±0.58%; the experimental data are represented by the correlation with $R^2 = 0.96$. The global RMS of the drop size in the sprays was found to increase with the global Sauter mean drop size, i.e., the larger the biggest drops, the wider the drop size spectra. The drop size spectra of the sprays investigated were modeled using a gamma distribution. For representing even higher-order moments of the experimental spectra well, the original version of the model distribution found in the literature had to be modified empirically so as to represent

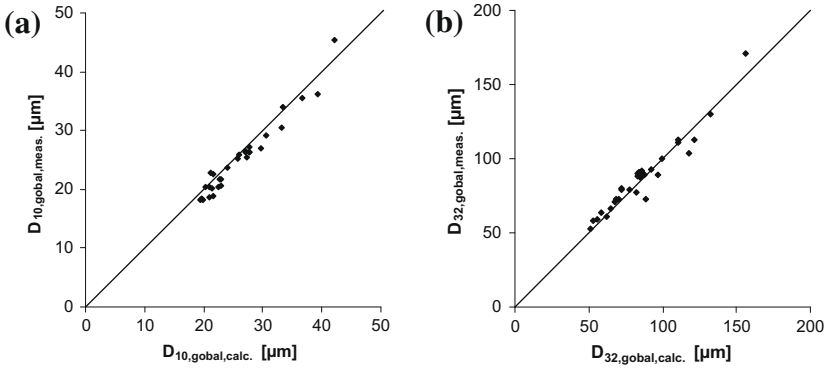

Fig. 17. Comparison of (a) the global number mean drop size $D_{10,global}$ and (b) the global Sauter mean drop size $D_{32,global}$ from the measurements and from the modified gamma distribution-based Probability Density Function (30) for the experiments in Tables 3 and 5. The individual values of the gamma distribution parameter ν and the parameters κ, C_1, and C_2 of the modified gamma distribution were obtained by fits to the corresponding experimental data.

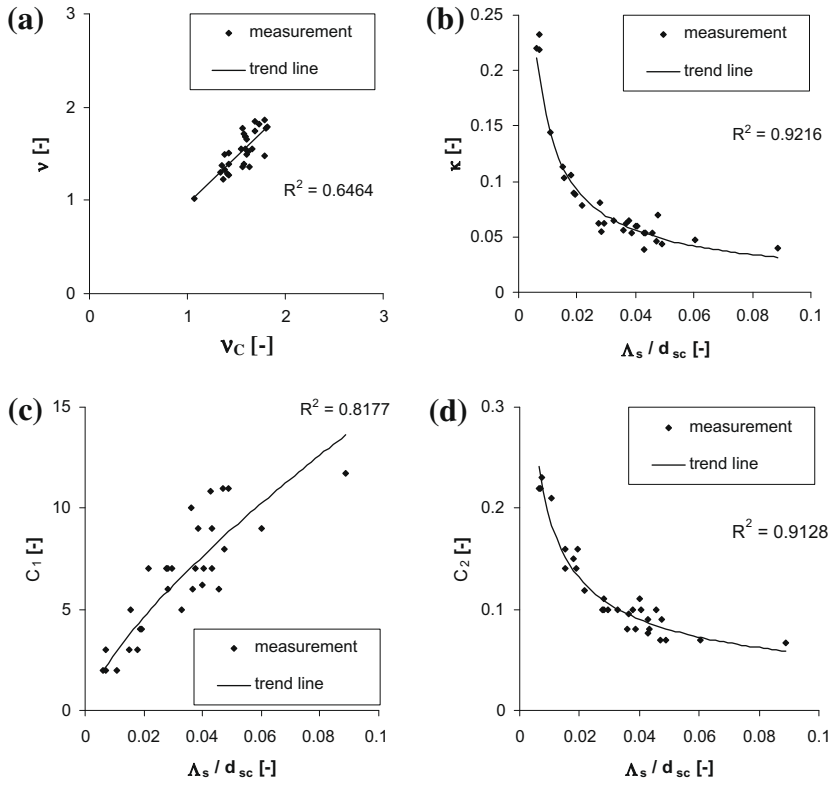

Fig. 18. Correlations for the four parameters of the modified gamma distribution. (a) Gamma distribution parameter ν, (b) parameter κ of the gamma distribution, and parameters (c) C_1 and (d) C_2. The quantity ν_C represents the right-hand side of Eq. (31).

the large drops in the sprays better. Correlations of the four parameters of the modified function with easily accessible properties of the spray experiments enable the drop size spectra of the sprays and their moments to be predicted with high accuracy. Input data needed are the liquid mass flow rate, the driving pressure difference, the sheet opening angle, density, dynamic viscosity, and surface tension of the liquid, the ambient gas density, and the swirl chamber and orifice diameters of the atomizer. The results pre-

Table 5
Measured global mean drop sizes and calculated drop size distribution parameters of the 30 experiments.

Experiment #	$D_{10,\mathrm{global}}$ (μm)	$D_{32,\mathrm{global}}$ (μm)	ν (–)	κ (–)	C_1 (–)	C_2 (–)
1	21.73	58.86	1.5517	0.2328	2	0.22
2	18.13	52.92	1.552	0.2196	2	0.22
3	34.00	130.63	1.301	0.0531	6	0.1
4	29.27	113.06	1.2334	0.06	6.19	0.11
5	18.11	58.17	1.2718	0.2185	3	0.23
6	20.57	92.62	1.3262	0.088	4	0.16
7	45.44	171.49	1.0267	0.0393	11.75	0.067
8	35.43	112.61	1.487	0.0473	9	0.07
9	26.42	90.74	1.3904	0.062	6	0.095
10	20.18	72.74	1.7783	0.0901	4	0.14
11	36.11	110.97	1.5014	0.07	8	0.09
12	20.42	66.46	1.3956	0.113	3	0.16
13	25.39	77.54	1.381	0.0807	6	0.11
14	26.37	100.02	1.284	0.0531	7	0.09
15	26.24	89.09	1.4716	0.0645	5	0.1
16	22.89	73.60	1.777	0.0391	10.86	0.077
17	20.35	61.74	1.861	0.0782	7	0.119
18	25.80	91.62	1.55	0.0439	11	0.07
19	18.66	80.05	1.6874	0.0616	7	0.1
20	23.79	80.91	1.6597	0.0557	10	0.08
21	18.90	73.60	1.5182	0.1437	2	0.21
22	30.51	103.58	1.7125	0.0593	7	0.1
23	27.02	89.31	1.6805	0.0641	7	0.1
24	18.43	63.88	1.8488	0.1029	5	0.14
25	21.77	71.00	1.74	0.1055	3	0.15
26	20.42	79.01	1.4857	0.0617	7	0.1
27	26.58	90.05	1.782	0.0532	9	0.08
28	27.26	91.43	1.8199	0.0537	9	0.08
29	25.27	88.76	1.3628	0.0458	11	0.07
30	22.53	88.04	1.3575	0.0546	7	0.1

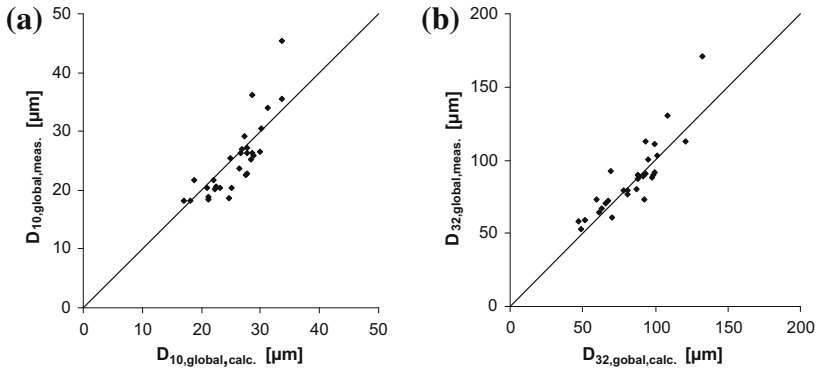

Fig. 19. Comparison of (a) the global number mean drop size $D_{10,\mathrm{global}}$ and (b) the global Sauter mean drop size $D_{32,\mathrm{global}}$ from the measurements and from the modified gamma distribution-based Probability Density Function (30) for the experiments in Tables 3 and 5. The four distribution parameters were calculated by the correlations (31)–(34).

sented here are valid for sprays from pressure-swirl atomizers with geometries comparable to the SDX atomizer series of Delavan, spraying into air at atmospheric conditions, in the following ranges of values of the influencing parameters: 141 kg/h $\leqslant \dot{m} \leqslant$ 538 kg/h, 7.5 bar $\leqslant \Delta p \leqslant$ 152 bar, 1201 kg/m^3 $\leqslant \rho \leqslant$ 1315 kg/m^3, 0.00869 Pas $\leqslant \mu \leqslant$ 0.1714 Pas, 0.0465 N/m $\leqslant \sigma \leqslant$ 0.072 N/m, 10.71 mm $\leqslant d_{\mathrm{SC}} \leqslant$ 11.85 mm, and 0.762 mm $\leqslant d_{\mathrm{Or}} \leqslant$ 1.778 mm. The findings of this work enable one to predict and design the drop size spectra of hollow-cone sprays, which is of importance for many applications.

Acknowledgment

Financial support of the present work by the Nestlé Product Technology Centre Konolfingen (Switzerland) in the frame of an R&D cooperation is gratefully acknowledged.

References

Babinsky, E., Sojka, P.E., 2002. Modeling drop size distributions. Prog. Energy Combust. Sci. 28, 303–329.
Bhatia, J.C., Durst, F., 1989. Comparative study of some probability distributions applied to liquid sprays. Part. Part. Syst. Char. 6, 151–162.
Bremond, N., Clanet, C., Villermaux, E., 2007. Atomization of undulating liquid sheets. J. Fluid Mech. 585, 421–456.
Clark, C.J., Dombrowski, N., 1972. Aerodynamic instability and disintegration of inviscid liquid sheets. Proc. R. Soc. Lond. A 329, 467–478.
Dahl, H.D., Muschelknautz, E., 1992. Atomization of liquids and suspensions with hollow cone nozzles. Chem. Eng. Technol. 15, 224–231.
Dexter, R.W., 2001. The effect of fluid properties on the spray quality from a flat fan nozzle. Pestic. Formulation Appl. Syst. 20, 27–43.
Dombrowski, N., Johns, W.R., 1963. The aerodynamic instability and disintegration of viscous liquid sheets. Chem. Eng. Sci. 18, 203–214.
Dorfner, V., Domnick, F., Durst, F., Köhler, R., 1995. Viscosity and surface tension effect in pressure swirl atomization. Atomization Spray 5, 261–285.
Dumouchel, C., 2006. A new formulation of the maximum entropy formalism to model liquid spray drop size distribution. Part. Part. Syst. Char. 23, 468–479.
Hewitt, A.J., 2008. Spray optimization through application and liquid physical property variables-I. Environmentalist 28, 25–30.
Lefebvre, A.H., 1989. Atomization and Sprays. Taylor and Francis, London, UK.
Li, X., Tankin, R.S., 1989. Prediction of the drop size and velocity distribution in a spray, based on the maximum entropy formalism. Part. Part. Syst. Char. 6, 17–27.
Li, X., Tankin, R.S., 1991. On the temporal instability of a two-dimensional viscous liquid sheet. J. Fluid Mech. 226, 425–443.
Marmottant, P., Villermaux, E., 2004. Fragmentation of stretched liquid ligaments. Phys. Fluids 16, 2732–2741.
Miller, P.C.H., Butler Ellis, M.C., 2000. Effects of formulation on spray nozzle performance for applications from ground-based boom sprayers. Crop Prot. 19, 609–615.
Mugele, R.A., Evans, H.D., 1951. Droplet size distributions in sprays. Ind. Eng. Chem. 43, 1317–1324.
Nonnenmacher, S., Piesche, M., 2000. Design of hollow cone pressure swirl nozzles to atomize Newtonian fluids. Chem. Eng. Sci. 55, 4339–4348.
Paloposki, T., 1994. Drop size distributions in liquid sprays. Acta Polytech. Sc., Mech. Eng. Ser. No. 114, Helsinki.
Richter, T., Glaser, H.W., 1987. Auslegung von Hohlkegel-Druckdüsen. Chem.-Ing.-Tech. 59, 332–334.
Saffman, M., 1987. Automatic calibration of LDA measurement volume size. Appl. Opt. 26, 2592–2597.
Schmidt, D.P., Nouar, I., Senecal, P.K., Rutland, C.J., Martin, J.K., Reitz, R.D., Hoffman, J.A., 1999. Pressure-swirl atomization in the near field. SAE Trans., J. Engine 108, 471–484.
Schütz, S., Breitling, M., Piesche, M., 2004. Atomization of suspensions with shear-thinning behaviour by aerodynamic wave breakup. Chem. Eng. Technol. 27, 619–624.
Sellens, R.W., Brzustowski, T.A., 1985. A prediction of the drop size distribution in a spray from first principles. Atomisation Spray Technol. 1, 89–102.
Senecal, P.K., Schmidt, D.P., Nouar, I., Rutland, C.J., Reitz, R.D., Corradini, M.L., 1999. Modeling high-speed viscous liquid sheet atomization. Int. J. Multiphase Flow 25, 1073–1097.
Sheng, H., Wu, D., Zhang, H., Wei, X., 2006. Viscosity, surface tension, and atomization of water–methanol and diesel emulsions. Atomization Spray 16, 1–13.
Sowa, W.A., 1992. Interpreting mean drop diameters using distribution moments. Atomization Spray 2, 1–15.
Squire, H.B., 1953. Investigation of the instability of a moving liquid film. Brit. J. Appl. Phys. 4, 167–169.
Villermaux, E., Marmottant, P., Duplat, J., 2004. Ligament-mediated spray formation. Phys. Rev. Lett. 92. No. 074501.
Villermaux, E., 2007. Fragmentation. Ann. Rev. Fluid Mech. 39, 419–446.
Walzel, P., 1998. Spraying and Atomizing of Liquids. Ullmann's Encyclopedia of Industrial Chemistry. Wiley-VCH, Weinheim, Germany.
Weber, C., 1931. Zum Zerfall eines Flüssigkeitsstrahles. Z. Angew. Math. Mech. 11, 136–154.
Xu, T.H., Durst, F., Tropea, C., 1993. The three-parameter log-hyperbolic distribution and its application to particle sizing. Atomization Spray 3, 109–124.